Two separate functions of NME3 critical for cell survival underlie a neurodegenerative disorder

Chih-Wei Chen[a], Hong-Ling Wang[a], Ching-Wen Huang[b], Chang-Yu Huang[c], Wai Keong Lim[a], I-Chen Tu[a], Atmaja Koorapati[a], Sung-Tsang Hsieh[d], Hung-Wei Kan[d], Shiou-Ru Tzeng[e], Jung-Chi Liao[f], Weng Man Chong[f], Inna Naroditzky[g], Dvora Kidron[h,i], Ayelet Eran[j], Yousif Nijim[k], Ella Sela[k], Hagit Baris Feldman[l], Limor Kalfon[m], Hadas Raveh-Barak[m], Tzipora C. Falik-Zaccai[m,n], Orly Elpeleg[o], Hanna Mandel[m,p,1], and Zee-Fen Chang[a,q,1]

[a]Institute of Molecular Medicine, College of Medicine, National Taiwan University, 10002 Taipei, Taiwan; [b]Department of Medicine, College of Medicine, National Taiwan University, 10002 Taipei, Taiwan; [c]Institute of Biochemistry and Molecular Biology, National Yang-Ming University, 11221 Taipei, Taiwan; [d]Institute of Anatomy and Cell Biology, College of Medicine, National Taiwan University, 10002 Taipei, Taiwan; [e]Institute of Biochemistry and Molecular Biology, College of Medicine, National Taiwan University, 10002 Taipei, Taiwan; [f]Institute of Atomic and Molecular Sciences, Academia Sinica, 10617 Taipei, Taiwan; [g]Department of Pathology, Rambam Health Care Campus, 31096 Haifa, Israel; [h]Department of Pathology, Meir Hospital, 44100 Kfar Saba, Israel; [i]Sackler School of Medicine, Tel Aviv University, 69978 Tel Aviv, Israel; [j]Department of Radiology, Rambam Health Care Campus, 31096 Haifa, Israel; [k]Pediatric and Neonatal Unit, Nazareth Hospital EMMS, 17639 Nazareth, Israel; [l]The Genetics Institute, Rambam Health Care Campus, 31096 Haifa, Israel; [m]Institute of Human Genetics, Galilee Medical Center, 22100 Nahariya, Israel; [n]The Azrieli Faculty of Medicine, Bar Ilan University, 13100 Safed, Israel; [o]Department of Genetic and Metabolic Diseases, Hadassah Hebrew University Medical Center, 91120 Jerusalem, Israel; [p]Metabolic Unit, Technion Faculty of Medicine, Rambam Health Care Campus, 31096 Haifa, Israel; and [q]Center of Precision Medicine, College of Medicine, National Taiwan University, 10002 Taipei, Taiwan

Edited by Christopher K. Glass, University of California, San Diego, La Jolla, CA, and approved November 26, 2018 (received for review November 4, 2018)

We report a patient who presented with congenital hypotonia, hypoventilation, and cerebellar histopathological alterations. Exome analysis revealed a homozygous mutation in the initiation codon of the *NME3* gene, which encodes an NDP kinase. The initiation-codon mutation leads to deficiency in NME3 protein expression. NME3 is a mitochondrial outer-membrane protein capable of interacting with MFN1/2, and its depletion causes dysfunction in mitochondrial dynamics. Consistently, the patient's fibroblasts were characterized by a slow rate of mitochondrial dynamics, which was reversed by expression of wild-type or catalytic-dead NME3. Moreover, glucose starvation caused mitochondrial fragmentation and cell death in the patient's cells. The expression of wild-type and catalytic-dead but not oligomerization-attenuated NME3 restored mitochondrial elongation. However, only wild-type NME3 sustained ATP production and viability. Thus, the separate functions of NME3 in mitochondrial fusion and NDP kinase cooperate in metabolic adaptation for cell survival in response to glucose starvation. Given the critical role of mitochondrial dynamics and energy requirements in neuronal development, the homozygous mutation in *NME3* is linked to a fatal mitochondrial neurodegenerative disorder.

NME3 | NDP kinase | mitochondrial fusion | neurodegeneration | metabolic adaptation

NMEs, nucleoside diphosphate (NDP) kinases, are highly conserved proteins in eukaryotes and are involved in different cellular processes (1, 2). NME1 to 10 in humans are encoded by 10 different genes. NME1 to 4, 6, and 7 have the catalytic function that transfers the terminal phosphate of a nucleoside triphosphate to a nucleoside diphosphate via histidine phosphorylation at the catalytic site, thereby equilibrating the NDP and NTP pools in a cell (3). A recent study has shown that NME1/2 interact with dynamin and NME4 with OPA1 (4). Dynamin and OPA1 are the GTPases that mediate endocytosis and mitochondrial fusion at the inner membrane, respectively. The complex formation of GTPases with NME increases GTP loading that activates these GTPases. Therefore, NME1/2 have a functional role in promoting dynamin-mediated endocytosis and NME4 in the OPA1-mediated mitochondrial fusion process at the inner membrane (4). As for NME3, it has been shown that NME3 participates in NME2/Gαβγ formation to control the activity of $G\alpha_s$ by GTP loading for regulating cAMP formation in cardiomyocytes (5).

Here we report on the identification of a homozygous deleterious mutation in the initiation codon of *NME3* in a patient with fatal infantile neurodegenerative disorder and prominent cerebellar involvement. This mutation caused deficiency in NME3 protein expression. In this study, our data revealed the subcellular localization of NME3 at the mitochondrial outer membrane dependent on its N-terminal region. The function of NME3 in mitochondria is not known. We then investigated how NME3 deficiency affects mitochondrial function in this patient's cells. The patient's fibroblasts exhibited abnormalities in mitochondrial dynamics which is controlled by balanced fusion and fission (6). In humans, the fusion and fission processes require four dynamin-related GTPases: MFN1, MFN2, OPA1, and DRP1. MFN1 and MFN2 mediate outer-membrane fusion followed by OPA1-dependent inner-membrane fusion to complete mitochondrial fusion, while DRP1 recruitment to the receptors triggers fission (7–10). In this study, we show that NME3 can interact with MFN1/2 and has a functional role in enhancing MFN1/2-mediated mitochondrial fusion. Therefore, the loss of NME3 in patient fibroblasts leads to the reduced rate of mitochondrial dynamics. Defects of mitochondrial fusion manifested by cerebellar disease were previously reported in humans (11) and in mice (12). Accordingly, our findings suggest that a homozygous mutation in *NME3* is linked to this mitochondrial neurodegenerative disorder.

Importantly, this investigation revealed the catalytic function of NME3 dispensable for mitochondrial dynamics. In nutrient

Significance

It is known that nutrient starvation stimulates mitochondrial fusion for cell survival. In this study, a homozygous mutation in the *NME3* gene, which encodes an NDP kinase, was identified in a fatal neurodegenerative disorder. Cells derived from the patient were deficient of NME3 and intolerant to glucose starvation. Patient cells were used to demonstrate that NME3 rescued cell survival by two separate functions, namely stimulation of mitochondrial fusion and NDP kinase activity. Since mitochondrial dynamics and energy efficiency are important for neuronal development, our data suggest a link between two functions of NME3 and a fatal neuronal disorder.

Author contributions: S.-T.H., S.-R.T., J.-C.L., O.E., H.M., and Z.-F.C. designed research; C.-W.C., H.-L.W., C.-W.H., C.-Y.H., W.K.L., I.-C.T., A.K., H.-W.K., S.-R.T., J.-C.L., and W.M.C. performed research; C.-W.C., H.-L.W., C.-W.H., S.-T.H., H.-W.K., S.-R.T., J.-C.L., I.N., D.K., A.E., Y.N., E.S., H.B.F., L.K., H.R.-B., T.C.F.-Z., O.E., H.M., and Z.-F.C. analyzed data; and H.M. and Z.-F.C. wrote the paper.

The authors declare no conflict of interest.

This article is a PNAS Direct Submission.

[1]To whom correspondence may be addressed. Email: h_mandel@rambam.health.gov.il or zfchang@ntu.edu.tw.

This article contains supporting information online at www.pnas.org/lookup/suppl/doi:10.1073/pnas.1818629116/-/DCSupplemental.

Published online December 26, 2018.

starvation, it is known that DRP1-mediated fission is suppressed, thereby increasing the tubular network of mitochondria due to fusion (13–15). In turn, the elongated mitochondria have higher efficiency in the respiratory electron transfer chain for sustaining cell viability. In this study, we found that after glucose starvation, mitochondria in the patient's cells became fragmented instead of elongated and died subsequently. By NME3-rescued experiment, we provide evidence that NME3 has two disparate functions: One is the stimulation of MFN-mediated mitochondrial elongation and the other is NDP kinase activity, both of which are coupled to support cell viability in response to glucose starvation.

Results

Pedigree and Clinical Features Associated with NME3 Homozygous Mutation. Two female siblings, whose parents are first-degree cousins (Fig. 1*A*), presented since birth with severe hypotonia, reduced spontaneous movements, and hypoventilation (for details, see *SI Appendix*, *Notes*). They died at age 3 to 4 mo. Magnetic resonance imaging of one studied baby revealed lesions in white matter and decreased cerebellar foliation (Fig. 1*B*). Brain autopsy of this baby showed vacuolar changes in the cerebral subcortical white matter and depletion of cerebellar Purkinje cells (Fig. 1*C*). We performed exome analysis of patient V-4 (Fig. 1*A*) under the hypothesis of a recessively inherited, rare, causal allele. The analysis yielded 47.7 million mapped reads with a mean coverage of 95×. Following alignment and variant calling, we performed a series of filtering steps and focused on Hg19 Chr16:1821535 A>G, p.Met1-Val in the *NME3* gene. Sanger sequencing confirmed the homozygous mutation in the initiation codon of *NME3* in both siblings and a carrier status of their parents (Fig. 1*D*); none of the 22 available asymptomatic relatives was homozygous for the mutant allele, but 17 of 22 were heterozygotes. Restriction fragment length polymorphism (RFLP) analysis confirmed the homozygous mutation of *NME3* of patient V-4 and heterozygous mutations of *NME3* of parents IV-6 and IV-7 (Fig. 1*E*).

The N-Terminal Region Is Essential for NME3 Mitochondrial Localization. Human NME3 protein consists of 169 amino acids. In addition to Met1, there are additional downstream methionine residues, Met85 and Met93. We thought to estimate the consequences of the Met1-Val mutation on the expression of NME3 protein in F741 fibroblasts derived from patient V-4 carrying the homozygous mutation in the initiation codon of *NME3*. However, we were unable to obtain specific anti-NME3 antibodies from either commercial sources or our in-house preparation. We then introduced a GTG mutation at ATG of the Met1 position in an expression vector of NME3-HA, in which HA was tagged at the C terminus of NME3. Of note, the second Met codon is at the position of Met85 in the ORF and the first ATG codon in out-of-frame reading is 29 nt downstream of Met85. Western blot analysis showed that Met^{1} (A>G) mutation led to no HA-tagged protein expression (Fig. 2*A*), probably due to the degradation of a short polypeptide or the lack of polypeptide maturation. In conclusion, F741 patient fibroblasts carrying the homozygous mutation are deficient of intact NME3.

To elucidate NME3 function in cell physiology, we first investigated the subcellular localization of NME3. Flag-wild-type (WT) NME3 was expressed under the Tet-on promoter. Confocal microscopy analysis of immunofluorescence (IF) staining of Flag-NME3 revealed the colocalization of NME3 with COX4, a mitochondrial marker. In contrast, the N-terminal 30-amino acid-deleted (ΔN)-NME3 mutant stayed all over the whole cell without colocalization with COX4 (Fig. 2*B*). Similar results were found in normal human BJ fibroblasts (Fig. 2*C*), and Western blotting showed the expression level of Flag-ΔN-NME3 mutant to be higher than Flag-WT-NME3 (*SI Appendix*, Fig. S1). Thus, NME3 is distributed to mitochondria dependent on the N-terminal region. We further performed superresolution microscopy analysis in human BJ fibroblasts expressing WT-NME3. The result showed that the major distribution of NME3 in mitochondria was at the outer membrane, as indicated by the costaining pattern with TOMM20, an outer-membrane protein (Fig. 2*D*). To confirm the outer-membrane

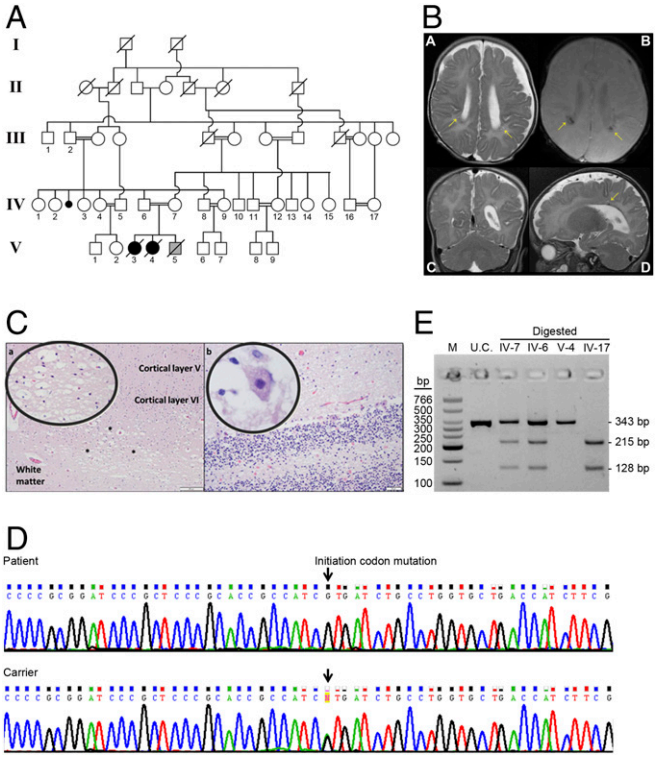

Fig. 1. Pedigree, segregation, sequencing analysis, and aberrations in the patient's brain. (*A*) Pedigree of the patient. Filled symbol, affected individuals (V-3 and V-4); symbol with a slash, deceased individual; the gray square with the diagonal line (V-5) indicates a male infant who died at age 6 wk of congenital diaphragmatic hernia and did not carry the mutation. The exome was sequenced in patient V-4. (*B*) In axial T2 and susceptibility-weighted imaging (SWI) images, coronal T2- and sagittal T2-weighted images at 12 wk of age. There are periventricular nonspecific punctate white matter lesions (arrows, A, B, and D) around the posterior aspect of the lateral ventricles that are visualized with low signal on SWI (B), suggestive for blood by-products. The lateral ventricles are asymmetric and there is excessive CSF around the frontal lobes, more on the left. The myelination pattern is age-appropriate. Of note, there is an impression of decreased cerebellar foliation (C and D). (*C*, *Left*) Cerebral hemisphere: vacuolated changes in subcortical white matter (asterisks), H&E, 40×. (Scale bars, 200 μm.) (*C*, *Left Inset*) Vacuolar changes, H&E 200×. (*C*, *Right*) Cerebellar cortex: depletion of Purkinje cells, H&E, 40×. (Scale bars, 50 μm.) (*C*, *Right Inset*) Cytoplasmic vacuolation of residual Purkinje cells. H&E, 400×. (*D*) Sanger sequencing of patient V-4 and the parent carrier. (*E*) Segregation analysis of p.Met1-Val in *NME3* by restriction fragment length polymorphism. A PCR product of 343 bp comprises the Met1-encoding region of the NME3 gene, and was digested using the *Fat*^{I} restriction enzyme. Methionine 1 codon (ATG) is recognized and digested by the enzyme to give 128- and 215-bp products while the genetic variant, comprising a valine codon (GTG), abolishes this restriction site. Therefore, the homozygous G allele at c.1 gives a 343-bp band only. Digested DNA samples of patient V-4, her heterozygous parents IV-6 and IV-7, and a homozygous wild type who is a healthy family member IV-17 are depicted. M, DNA marker; U.C., uncut DNA.

localization of NME3, we isolated mitochondria for proteinase K digestion. Flag-NME3, similar to other outer-membrane proteins such as MFN1, MFN2, and TOMM20, was susceptible to proteinase K digestion, while matrix protein COX4 was unaffected by the digestion unless the mitochondrial membrane was disrupted by Triton X-100 (Fig. 2*E*). These results led us to speculate that the mitochondria in the patient's cells were affected by the loss of intact *NME3*.

NME3 Regulates MFN-Mediated Mitochondrial Fusion. NME4 located in mitochondrial intermediate space interacts with OPA1 to mediate inner-membrane fusion. Since mitochondrial outer-membrane fusion precedes inner-membrane fusion (2, 16), we then examined the

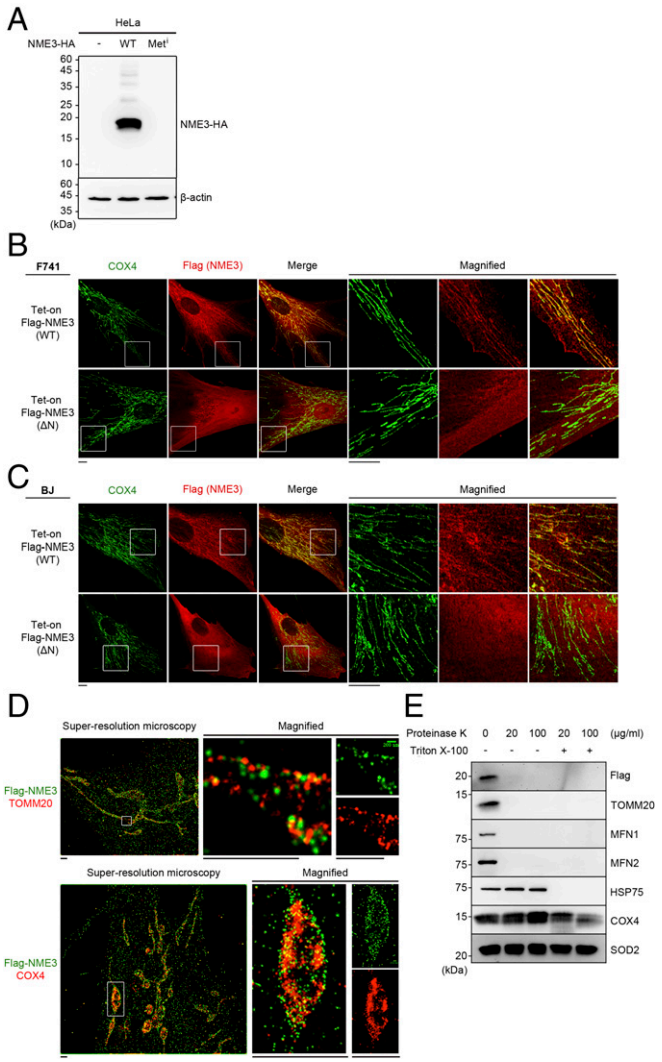

Fig. 2. N-terminal region is essential for NME3 mitochondrial localization. (*A*) HeLa cells were transfected with an expression vector of WT-HA or Met^{i}-HA. Cells were harvested for Western blotting by HA antibody. (*B* and *C*) F741 (*B*) and BJ (*C*) fibroblasts were infected with lentivirus of Tet-on Flag-WT or N-terminal 30-amino acid-deleted mutant (ΔN) NME3 for 48 h, followed by doxycycline (5 μg/mL) induction for 16 h. Cells were fixed for immunofluorescence staining by anti-Flag and anti-COX4 antibodies. (Scale bars, 10 μm.) (*D*) dSTORM superresolution images of BJ cells expressing Flag-WT-NME3. The images show the distribution pattern of TOMM20 and COX4 with Flag-NME3. (Scale bars, 1 μm.) (*E*) HeLa cells expressing Tet-on Flag-NME3 (WT) were treated with doxycycline (4 μg/mL) induction for 12 h. Isolated mitochondria fractions were incubated with proteinase K as indicated in the presence and absence of 1% Triton X-100 to permeabilize the mitochondrial inner membrane for 30 min. The expression of the mitochondrial outer-membrane proteins TOMM20 and MFN1/2, mitochondrial inner-membrane protein COX4, and mitochondrial matrix proteins HSP75 and SOD2, and Flag-NME3 were analyzed by Western blotting.

effect of NME3 knockdown on mitochondrial dynamics in BJ fibroblasts by performing the mito-Dendra2 reporter assay. Upon site-specific excitation of mito-Dendra2 to red fluorescence in the region of interest (ROI) (17), mitochondrial fusion allowed unexcited green fluorescence-labeled mitochondria merging with red fluorescence. Cells expressing the mito-Dendra2 reporter were preincubated with cycloheximide before site-specific excitation in ROIs of isolated mitochondria. As shown in Fig. 3 *A* and *B* (Movies S1 and S2), the rate of fluorescence change in NME3 knockdown cells was much slower than that in control cells. Similar results were also observed in HeLa cells (*SI Appendix*, Fig. S2 and Movies S3 and S4). Thus, the depletion of NME3 slows the mitochondrial dynamics.

We further assessed the molecular relationship between NME3 and mitochondrial outer-membrane fusion GTPases, MFN1 and MFN2. Flag-tagged WT- and ΔN-NME3 were coexpressed with Myc-His-MFN1 or Myc-His-MFN2 for coimmunoprecipitation (IP) in HeLa cells. The IP-Western showed the complex formation of MFN1 and MFN2 with WT- but not ΔN-NME3 (Fig. 3*C*). The immunoprecipitation of Flag-NME3 also pulled down endogenous MFN1 in HEK293T cells, confirming their complex formation (*SI Appendix*, Fig. S3). By the proximity ligation assay (PLA), we observed the in vivo interaction of NME3 with MFN1 and MFN2 (Fig. 3*D* and *SI Appendix*, Fig. S4*A*), while little PLA signal in the cells was depleted of MFN1 or MFN2 (*SI Appendix*, Fig. S4*B*). Other mitochondrial outer-membrane proteins, TOMM20 and DRP1 (18), had little PLA signal with Flag-NME3. It is likely that the function of NME3 in mitochondrial fusion activity involves the interaction with mitofusins.

NME3 Rescues Mitochondrial Fusion Independent of NDP Kinase Activity. The NDP kinase activity of NME4 has been shown to be critical for OPA-mediated mitochondrial fusion. We then tested whether the stimulation of mitochondrial fusion by NME3 is dependent on the NDP kinase activity of NME3. To this end, we first tested the effect of H135Q mutation on NDP kinase activity of NME3. Recombinant His-WT- and -H135Q-NME3 proteins were purified for NDP kinase activity assay. The result showed that the

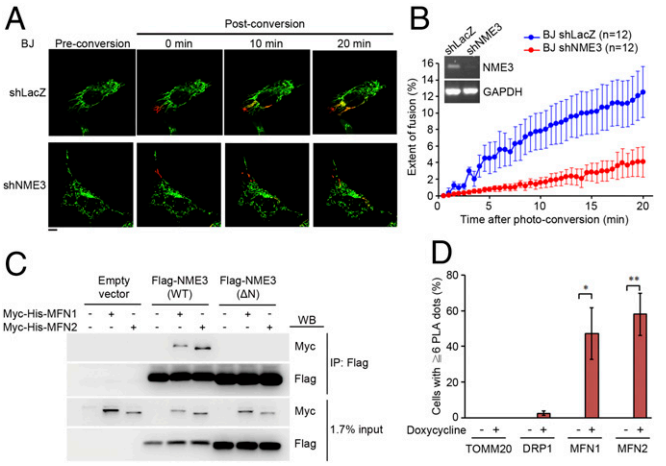

Fig. 3. Patient cells are deficient in NME3-dependent mitochondria dynamics. (*A*) Normal BJ fibroblasts were infected with shLacZ or shNME3 virus followed by transfection with mito-Dendra2. Cells were pretreated with cycloheximide (30 μg/mL) for 30 min. Laser activation was applied to allow green-to-red photoconversion of mito-Dendra2. Thereafter, mitochondria in the entire cell were monitored at intervals of 30 s for 20 min. The generation of yellow fluorescence indicates the fusion of red mito-Dendra2 with non-converted green mito-Dendra2. (Scale bar, 10 μm.) (*B*) Quantification of mitochondrial fusion. The increased area in yellow fluorescence relative to the green fluorescence of mito-Dendra2 in the entire cell was quantitated by the colocalization coefficient at each time point. Data are shown as mean ± SEM (BJ shLacZ, $n = 12$; BJ shNME3, $n = 12$). (*B*, *Inset*) NME3 knockdown by RT-PCR. (*C*) The N-terminal region-dependent coimmunoprecipitation of Flag-NME3 with Myc-His-MFN1/MFN2. HEK293T cells were transfected with His-Myc-MFN1 or His-Myc-MFN2 together with Flag-WT or -ΔN NME3 as indicated. The lysates were immunoprecipitated using M2 beads, followed by Western blotting (WB). (*D*) Proximity ligation assay for Flag-NME3 interaction with endogenous MFN1/MFN2 in vivo. BJ cells infected with lentivirus of Tet-on-Flag-NME3 were treated with doxycycline (1 μg/mL) overnight and fixed for staining with antibodies against Flag/MFN1, Flag/MFN2, Flag/DRP1, and Flag/TOMM20. Following ligation and polymerization reactions, cells were stained with PLA probe. Data represent mean ± SEM; 150 cells were counted in three independent experiments. $^{*}P < 0.05$, $^{**}P < 0.01$ based on Student's *t* test.

H135Q mutant lacks NDP kinase activity (Fig. 4*A*). We then infected patient F741 cells with lentivirus of Tet-on Flag-WT- and -H135Q-NME3 for mito-Dendra2 reporter analysis. Of note, all cells were treated with doxycycline for comparison to exclude the potential effect of doxycycline in mitochondria (19). Patient cells showed little fusion activity in the analysis. WT-NME3 expression clearly increased fusion activity in these cells (Fig. 4 *B* and *C* and Movies S5–S7). However, expression of H135Q (HQ) also restored mitochondrial fusion activity. Western blot analysis showed that expression of WT and H135Q-NME3 did not change the levels of MFN1/2, DRP1, and OPA1 in patient F741 cells (Fig. 4*D*). The stimulation of mitochondrial dynamics by expression of WT-NME3 in patient cells suggests that the initiation-codon mutation in *NME3* causes a defect in mitochondrial dynamics. Importantly, these data indicate that the catalytic activity of NME3 is dispensable for its functionality in mitochondrial dynamics.

Mitochondrial Changes Due to the Loss of NME3 in Patient Cells. Compelling evidence has shown that mitochondrial dynamics by fusion and fission governs mitochondrial morphology (20–22). We then examined mitochondrial morphology by electron microscopy (EM) analysis in patient cells with and without Tet-on NME3 virus infection. With doxycycline treatment, EM micrographs showed short mitochondria in patient F741 cells, whereas WT or H135Q-NME3–expressing cells had more mitochondria with elongated morphology with more prominent cristae area (Fig. 5*A*). MitoSOX staining results indicated that patient F741 cells had higher mitochondrial oxidative stress than F689 cells derived from a healthy individual.

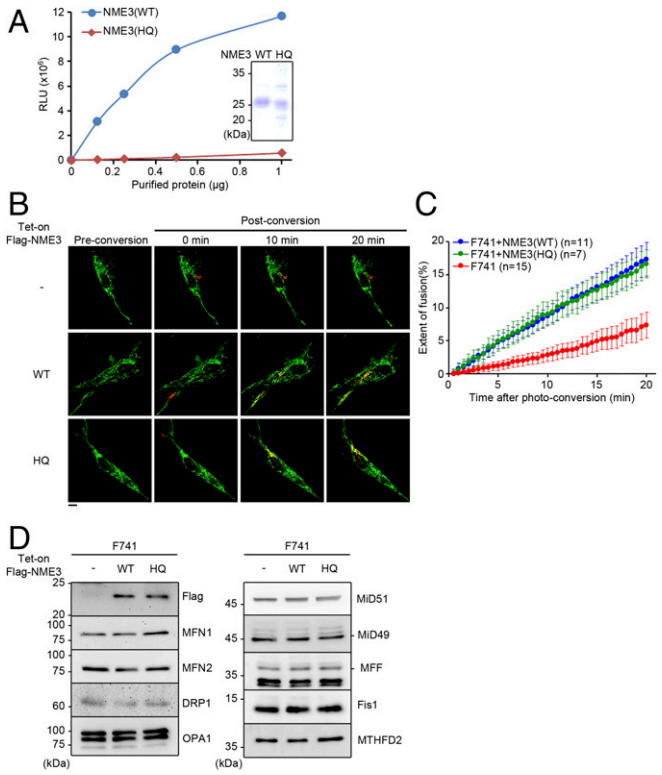

Fig. 4. Wild-type and NDPK-dead NME3 expression restores mitochondrial dynamics in patient cells. (*A*) NDPK activities of purified His-WT and -H135Q (HQ) of NME3. The indicated amounts of purified proteins were incubated in reaction buffer containing ADP and UTP coupled with the luciferase assay to measure ATP formation. RLU, relative light unit. (*B–D*) F741 cells infected without or with lentivirus of Tet-on Flag-WT or H135Q-NME3 for 2 d were transfected with mito-Dendra2 plasmid and doxycycline treatment overnight for (*B*) photoconversion, (*C*) quantification of fluorescence change as described in the legend to Fig. 3*B*, and (*D*) expression of proteins responsible for mitochondrial fusion and fission in these cells by Western blot. Data are shown as mean ± SEM. (Scale bar, 10 μm.)

WT or H135Q-NME3 expression decreased mitochondrial oxidative stress in patient F741 cells (Fig. 5*B*). This is consistent with the notion that the increase in the assembly of electron chain transfer complexes by mitochondrial fusion activity has contribution to minimizing electron leakage that generates mitochondrial reactive oxygen species (21–23). Mitochondrial fusion and fission are controlled by GTPases, MFN1/2, OPA1, and DRP1. Western blot analysis showed no significant difference in levels of MFN1/2, DRP1, and OPA1 in patient F741 and normal F689 cells (Fig. 5*C*). A recent report has shown that increasing mitochondrial copy number overcomes the pathogenic phenotype by mutation load of mitochondria (23). We then analyzed mitochondrial DNA copy number. The results showed that mitochondrial DNA copy number was higher in F741 cells compared with that in F689 and F741 rescued by WT or H135Q NME3 expression (Fig. 5*D*). We also performed analysis of oxygen consumption rate. Data of basal and ATP-linked oxygen consumption rate (OCR) were similar in patient cells with and without WT- or H135Q-NME3 expression. However, the maximal capacity of OCR in patient cells was higher than the rescued cells (Fig. 5*E*). Western blot of oxidative phosphorylation (OXPHOS) complexes showed that the amounts of complexes I, II, and IV relative to V were higher in patient cells without NME3 expression (Fig. 5*F*). Accordingly, it is possible that the increase in mitochondrial copy number in F741 patient cells is a compensatory mechanism aiming at normalization of the mitochondrial respiratory function.

Glucose Starvation Causes Patient Cell Mitochondrial Fragmentation and Cell Death. It is known that metabolic stress leads to mitochondrial fusion, which enhances electron transfer chain function with an elongated network and is essential for cell survival (13, 14). In control F689 cells, as expected, glucose starvation increased mitochondrial elongation with tubular morphology. Oppositely, in F741 cells, we observed increases in intermediate and fragmented mitochondria (Fig. 6 *A* and *B*). After glucose starvation for 32 h, F689 cells were viable while F741 cells died (Fig. 6*C*).

The Expression of WT and Catalytic-Dead NME3 Restores MFN1-Dependent Mitochondrial Elongation After Glucose Starvation. We further tested whether NME3 could rescue glucose starvation-induced mitochondrial fusion in patient cells. Again, cells were infected with lentivirus of Tet-on Flag-NME3 variants. After doxycycline treatment and glucose starvation for 24 h, we found that induction of WT- or H135Q-NME3 in F741 patient cells significantly increased tubular mitochondria fraction (Fig. 7*A*), while ΔN mutant expression caused more fragmented mitochondria. WT- or H135Q-NME3 also rescued mitochondrial elongation in BJ cells depleted of NME3 (*SI Appendix*, Fig. S5). Knockdown of MFN1 reversed mitochondrial elongation stimulated by NME3, indicating that NME3 acts up-stream of MFN1-mediated fusion after glucose starvation (Fig. 7*B*). Here, we concluded that the loss of glucose starvation-induced mitochondrial elongation in F741 patient fibroblasts is due to NME3 deficiency. We also examined the respiratory function of F741 by OCR measurement under the glucose-starved conditions before cells were exhausted. Surprisingly, the basal, ATP-linked, and maximal OCR data were similar in F741 and WT and H135Q-NME3–expressing cells (Fig. 7*C*). It is likely that mitochondrial fragmentation in F741 cells did not impair the overall respiratory function of mitochondria under the condition of glucose starvation.

Separate Functions of NME3 in Mitochondrial Fusion and NDP Kinase Sustain Viability in Response to Glucose Starvation. We further asked the question of whether NME3 is sufficient to support the viability of F741 cells in response to glucose starvation. It appeared that only expression of WT-NME3 was able to rescue the survival of F741 cells under a condition of glucose deprivation (Fig. 8*A*). This suggests that the N terminus and catalytic function of NME3 are required to sustain viability. Apparently, under glucose starvation conditions, the acquisition of mitochondrial fusion by catalytic-dead NME3 is insufficient to support metabolic adaptation for survival.

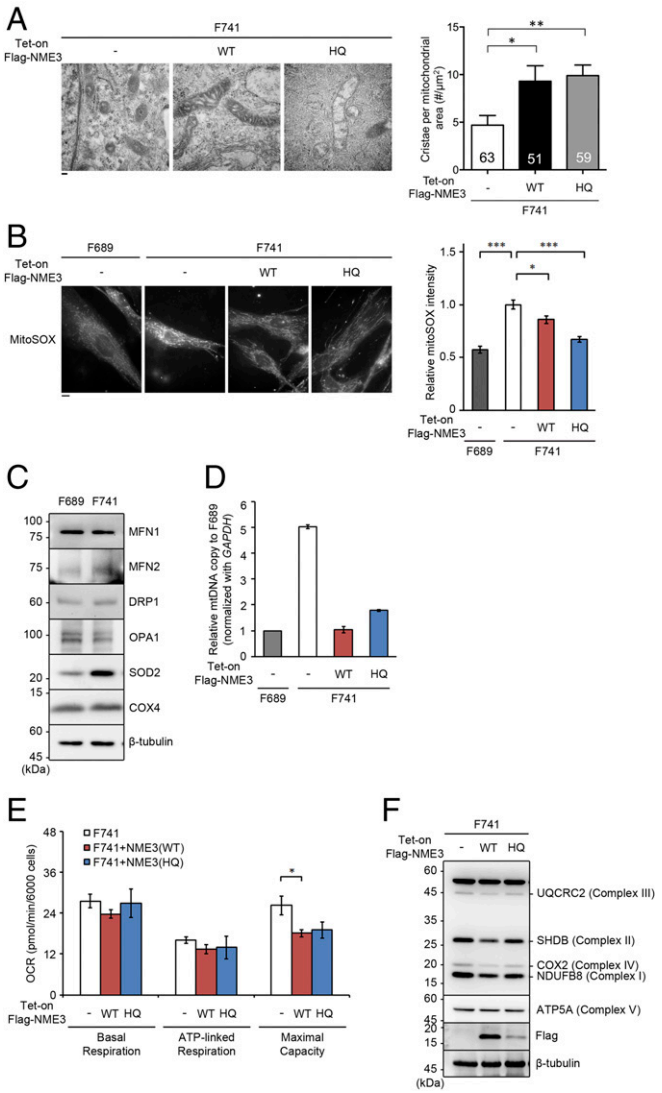

Fig. 5. Mitochondrial parameters reversed by NME3 expression in patient cells. (*A*) F741 cells were infected with lentivirus of Tet-on Flag-WT- and -H135Q (HQ)-NME3. After incubation with doxycycline for 2 d, cells were fixed for electron microscopy. (*A*, *Left*) Representative EM images. (*A*, *Right*) Relative mitochondrial cristae density, which was expressed as the number of cristae per unit area of mitochondria (numbers per μm^2). (Scale bar, 100 nm.) (*A*, *Right*) Quantitation results were expressed as the mean ± SEM and analyzed in Prism (GraphPad Software). One-way ANOVA with Dunnett's post hoc test was used in the analysis of mitochondrial cristae density. $^*P < 0.05$, $^{**}P < 0.01$. (*B*) Levels of mitochondrial oxidative stress in F689 and F741 expressing Flag-WT and H135Q (HQ)-NME3 were measured by MitoSOX staining. (Scale bar, 10 μm.) MitoSOX intensity was quantitated in more than 40 cells by ImageJ ($n = 3$). $^*P < 0.05$, $^{***}P < 0.001$ based on Student's *t* test. (*C*) The protein levels of MFN1/2, DRP1, OPA1, SOD2, COX4, and β-tubulin in F689 and F741 were analyzed by Western blotting. (*D*) Mitochondrial DNA (mtDNA) copy number in F689 and F741 expressing Flag-WT- and -H135Q (HQ)-NME3 was analyzed by quantitative real-time PCR of *mitochondria encoded NADH dehydrogenase 1* gene and nuclear *GAPDH* DNA. Relative mtDNA copy number normalized by nuclear DNA (*GAPDH*) is shown ($n = 2$). (*E*) Oxygen consumption rate of F741 expressing WT- and HQ-NME3 detected by Seahorse XFe24 Cell Mito Stress Test Kit (Agilent Technologies). Data represent mean ± SEM from three independent experiments. $^*P < 0.05$ compared with non-F741 control cells based on Student's *t* test. (*F*) The levels of oxidative phosphorylation proteins by Western blotting.

The measurement of the cellular ATP levels in these cells showed that only WT expression was able to sustain ATP production after glucose starvation (Fig. 8*B*). Thus, the catalytic activity of NME3 is still critical for bioenergetics under glucose-starved conditions. NME3 is a histidine kinase. We further examined the difference in histidine phosphorylation in these cells before cell exhaustion under glucose starvation. It has been shown that 1-pHis and 3-pHis antibodies are able to detect heat-sensitive histidine phosphorylation of proteins by Western blots (24). By this method, we found that heat-sensitive 1-His phosphorylation was detected in WT but not HQ-NME3 expressed in glucose-starved F741 fibroblasts, indicating WT retains phospho-transfer capacity under the condition (Fig. 8*C*). However, we were unable to detect any difference in 3-pHis staining in these samples (data not shown). Considering 1-His phosphorylation in active NME1 and 2, WT-NME3 is also active in 1-His phosphorylation under glucose-starvation conditions. Since the N-terminal region-deleted NME3 mutant defective in mitochondrial elongation also did not sustain cell viability, these data imply that cell survival under glucose starvation requires two different functions of NME3.

NME3 Stimulates Mitochondrial Elongation Dependent on Oligomerization Activity. We further generated an NME3 mutant defective in mitochondrial fusion but retaining mitochondrial localization. NME3 is a hexamer protein, in which the N terminus is required for anchoring to the outer membrane. It is possible that the oligomerization of

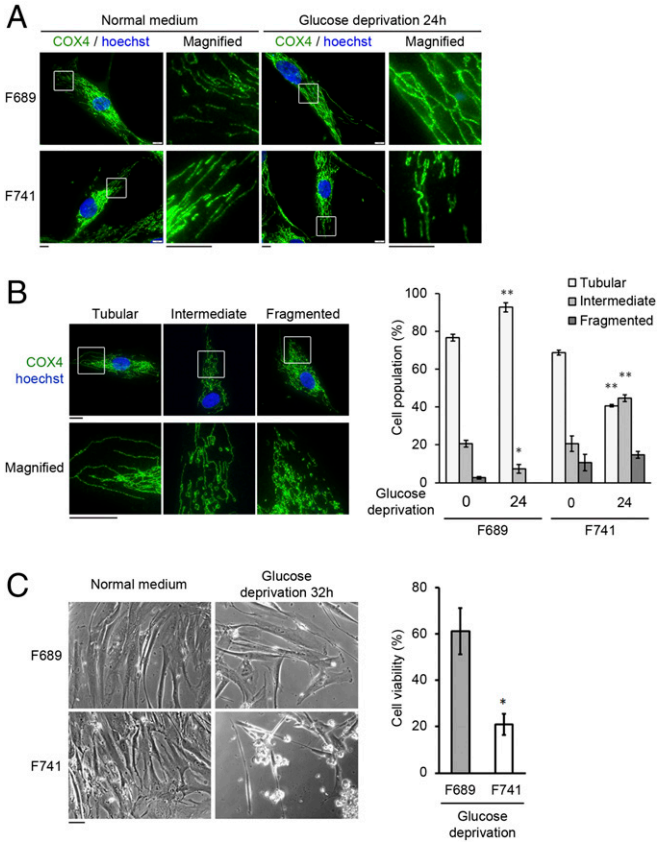

Fig. 6. Glucose starvation caused patient cell mitochondrial fragmentation and cell death. (*A*) Representative images of mitochondrial morphology of F689 and F741 incubated in normal and glucose-deprived medium for 24 h are shown. Cells were fixed for IF staining by anti-COX4 antibody. (Scale bars, 10 μm.) (*B*) Mitochondria in tubular, intermediate, and fragmented structures (*Left*) were counted. (Scale bars, 10 μm.) More than 80 cells were quantitated in each experiment ($n = 3$). $^*P < 0.05$, $^{**}P < 0.01$ compared with nondeprived controls based on Student's *t* test. (*C*) Phase-contrast images of F689 and F741 cells in the presence or absence of glucose-deprived medium for 32 h are shown. (Scale bar, 50 μm.) The percentage of surviving cells was analyzed by Trypan blue staining in three independent experiments. $^*P < 0.05$ based on Student's *t* test.

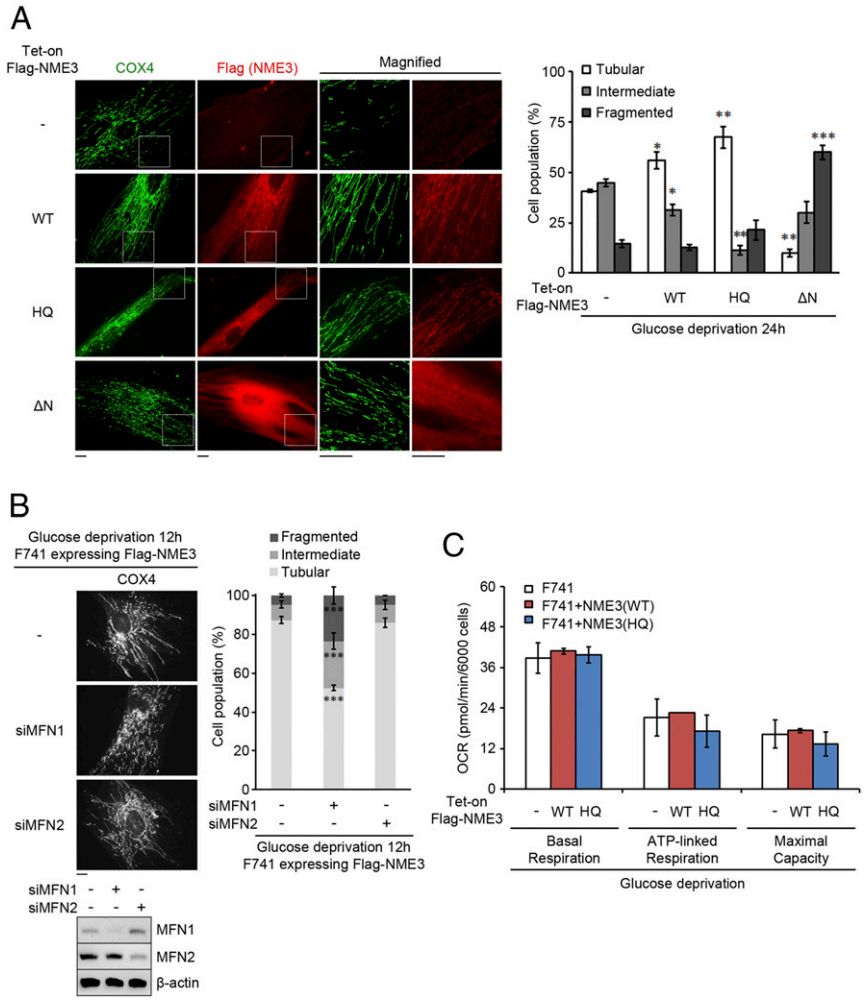

Fig. 7. NME3 rescues glucose starvation-induced mitochondrial elongation independent of NDPK activity. (*A*) Representative images of mitochondrial morphology of F741 expressing Tet-on Flag-WT, -HQ, and ΔN-NME3 are shown. All cells were treated with doxycycline for 24 h and incubated in glucose-deprived medium for another 24 h. Cells were fixed for IF staining by anti-COX4 and anti-Flag antibodies. Representative images are shown (*Left*). (Scale bars, 10 μm.) Mitochondria in tubular, intermediate, and fragmented structures were quantitated in more than 150 cells ($n = 3$). $^*P < 0.05$, $^{**}P < 0.01$, $^{***}P < 0.001$ based on Student's *t* test. (*B*) F741 expressing Tet-on Flag-WT NME3 were transfected with siMFN1 or siMFN2 as indicated and incubated in glucose-free medium for 12 h, followed by COX4 IF staining. (*B*, *Left*) Representative images of mitochondrial morphology are shown. (Scale bar, 10 μm.) (*B*, *Right*) Quantitation of cell fractions containing tubular, intermediate, and fragmented mitochondria; 150 cells were counted ($n = 3$). $^{***}P < 0.001$ based on Student's *t* test. (*B*, *Bottom*) Western blotting of MFN1 and MFN2 knockdown. (*C*) Oxygen consumption rate of F741, and F741 expressing WT- and HQ-NME3 under a condition of glucose deprivation overnight. OCR assays were performed in glucose/pyruvate-free medium. Data were from three independent experiments.

NME3 on the outer membrane plays a critical role in facilitating MFN1/2-mediated mitochondrial fusion. We examined the oligomerization interface of NME3 subunits by structural analysis (Fig. 9*A*), which indicated that Glu40 forms a salt bridge with Arg43 and hydrogen bonds contributed from Glu40/Glu46 in the interface. Introduction of the mutation at E40/E46 to D40/D46 (E40/46D) attenuated the oligomerization capacity of purified NME3, as manifested by the reduction in oligomerization in the cross-linking experiment (Fig. 9*B*). We further tested the rescue effect of this mutant in F741 cells. Unlike WT-NME3, expression of the E40D/E46D mutation in patient cells rescued neither mitochondrial elongation nor viability in patient cells under glucose-starved conditions (Fig. 9 *C*–*E*). Thus, the function of NME3 in stimulation of mitochondrial elongation is dependent on their oligomerization on the outer membrane of mitochondria.

Discussion

Exome analysis in a single patient who suffered from congenital hypotonia and hypoventilation revealed a homozygous mutation in the initiation codon of *NME3* gene, which encodes a mitochondrial NDP kinase. The homozygous mutation in this patient leads to the loss of intact NME3 protein. Although NME3 is localized on mitochondria, our knowledge of its mitochondrial function is limited. The patient's cells revealed normal respiratory function of the mitochondria. However, the mitochondrial fusion rate was slow and electron microscopy findings revealed abnormal cristae morphology. These abnormalities were rescued by expression of wild-type NME3. Even more so, our findings that NME3 knockdown in normal human fibroblasts and in HeLa cells resulted in reduced rates of mitochondrial fusion strengthen our suggestion that the homozygous initiation-codon mutation of the *NME3* gene in the patient's fibroblasts leads to abnormality in mitochondrial dynamics.

It has been shown that NME4, located in the intermediate space of mitochondria, is associated with OPA1, which gives the advantage of increasing local GTP supply by NME4 for OPA1 activation (4). In this study, we showed NME3 capable of interacting with MFN1/2. However, NME3-mediated enhancement of mitochondrial fusion is not through increasing GTP loading, because the

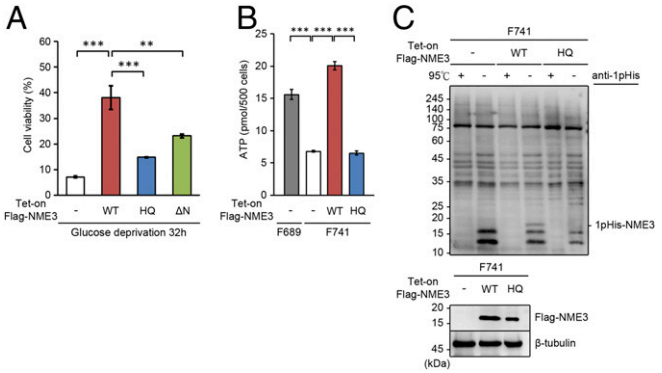

Fig. 8. NDPK function of NME3 is essential for sustaining viability and ATP production under glucose starvation. (*A*) Cell viability of F741 expressing Tet-on Flag-WT, -H135Q (HQ), and ΔN-NME3 in glucose-deprived medium for 32 h is shown. Data represent mean ± SEM from three independent experiments. $^{**}P < 0.01$, $^{***}P < 0.001$ based on Student's *t* test. (*B*) Cellular levels of ATP in F689 and F741 cells expressing Tet-on Flag-WT and H135Q (HQ)-NME3 were measured after being glucose-deprived for 24 h. Results are shown as mean ± SEM ($n = 3$). $^{***}P < 0.001$ based on Student's *t* test. (*C*) After glucose deprivation for 16 h, F741 cells expressing Tet-on Flag-WT and H135Q (HQ)-NME3 were harvested in SDS/PAGE sample buffer with or without heating at 95 °C for Western blotting by using 1-pHis antibody.

catalytic-dead mutant of NME3 was capable of rescuing the fusion activity and elongation of mitochondria in response to glucose deprivation in patient cells. Of note, knockdown of MFN1 in patient cells expressing NME3 still caused mitochondrial fragmentation, indicating that NME3 acts upstream of the MFN1-mediated fusion process to increase the fusion rate, resulting in an elongated mitochondrial network in glucose-starved cells. Since NME3 is a hexamer protein with the N-terminal region binding to the mitochondrial outer membrane, we proposed that it might have a function tethering the mitochondrial membrane via oligomerization. Together with MFN1 interaction, the oligomerization of NME3 would increase the rate of MFN1-mediated mitochondrial fusion. In support of this hypothesis, the E40D/E46D mutant with reduced capacity in oligomerization was unable to rescue mitochondrial elongation and viability under glucose deprivation.

Importantly, this study found that the catalytic function of NME3 is still required for the survival of patient cells under glucose-starved conditions. Therefore, in addition to mitochondrial fusion, the catalytic function of NME3 is essential for adaptation to glucose-starvation stress. It has been reported that acute glucose deprivation leads to AMPK activation to trigger lipophagy of lipid droplets for energy production (25). The mitochondrial tubular network promotes the close proximity of lipid droplets for fatty acid trafficking, thereby increasing the efficiency of beta oxidation and ATP generation (26). Recent studies have emerged showing reversible histidine phosphorylation of a variety of proteins in metabolic pathways by NDP kinases or NMEs in mammalian cells (27). It remains unknown whether kinase activity of NME3 in supporting cell survival in response to glucose starvation is through direct ATP formation or participation in nutrient utilization.

Fibroblasts may not reflect the devastating effect of mitochondrial dysfunction on dynamics. However, in neurons, the energy demand for electrical excitability and synaptic transmission relies on mitochondrial motility across long distances, which is closely associated with mitochondrial dynamics (28). It has been reported that cerebellar Purkinje neurons, unlike embryonic fibroblasts, cannot survive MFN2 removal (10, 12). Complete absence of MFN2 results in embryonic lethality largely attributed to placental insufficiency (10). Conditionally inactivated MFN2 mice show severe defects in movement and balance with uncoordinated limb movements and are markedly runted, possibly due to feeding problems secondary to their movement disorder. Upon examination, the sole abnormality in these animals is a severe defect in the postnatal growth of the cerebellum. This is attributed to Purkinje dendrites, which grow poorly, are less branched, and have fewer spines, and to a widespread loss of Purkinje cell bodies. The primary event is the abnormal clustering of mitochondria in the Purkinje cell body and its failure to enter the dendritic tracts. This process is accompanied by increased apoptosis of the granule cells, likely secondary to insufficient trophic support from Purkinje cells (12). Of interest, homozygosity for an Ashkenazi founder mutation in *THG1L*, encoding a guanine nucleotide exchange factor for MFN2, manifests solely by cerebellar atrophy (11). In this study, our investigation provides evidence for the critical role of NME3 upstream of MFN-mediated mitochondrial fusion. In accordance with the dysfunction in mitochondrial dynamics, the patient's clinical course and the severe loss of Purkinje cells are indicative of the grave consequences of the initiation-codon mutation in NME3. The development of the cerebellum in humans occurs with some delay in relation to the cerebrum. This delay in cerebellum linear size growth is observed until the fifth month of gestation, with a subsequent doubling of mass between the 19th and 37th weeks of fetal life (29). Later, the cerebellum continues to develop dynamically and doubles its mass in relation to the cerebrum mass from 1:25 at the moment of birth up to 1:10 to 1:15 in adult individuals. Thus, a defect in cerebellar growth may start in utero but manifest only after birth. Accordingly, the histopathological finding of depletion of cerebellar Purkinje cells combined with the fatal neurodegenerative progression of the disease underscore the profound effect of the homozygous mutation of

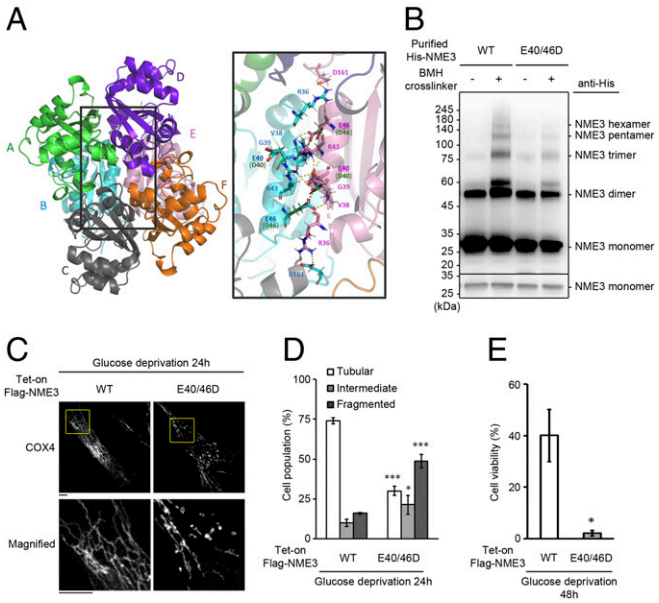

Fig. 9. Role of oligomerization of NME3 in stimulation of mitochondrial elongation and cell viability. (*A*) Cartoon representation of the hexameric human NME3 structure (Protein Data Bank ID code 1ZS3); NME3 subunits are color-coded. The region outlined by the rectangle is used for close-up views (*Right*). Close-up views of an extensive network of interactions between the NME3 monomers (subunits B and E). Nitrogen and oxygen atoms are labeled blue and red, respectively. The electrostatic contacts in the interfaces are as follows: The side chain of Glu46 forms hydrogen bonds with the backbone nitrogens of Val38 and Gly39; the side chain of Glu40 forms a salt bridge with Arg43. (*B*) Oligomerization of purified His-NME3 WT and E40/46D mutant by BMH cross-linking. (*C* and *D*) F741 cells expressing Flag-WT- and E40/46D-NME3 in glucose-deprived medium for 24 h were fixed for IF staining by using anti-COX4 antibody. (*C*) Representative images are shown. (Scale bars, 10 μm.) (*D*) Mitochondria in tubular, intermediate, and fragmented structures were quantitated in more than 150 cells ($n = 3$). $^{*}P < 0.05$, $^{***}P < 0.001$ based on Student's *t* test. (*E*) Cell viability of F741 expressing Tet-on Flag-WT and E40/46D-NME3 in glucose-deprived medium for 48 h is shown. Data represent mean ± SEM from three independent experiments. $^{*}P < 0.05$ based on Student's *t* test.

NME3. These findings are not only useful for the genetic counseling of affected families but also highlight the important function of NME3 in mitochondria.

Materials and Methods

Human Specimens and Whole-Exome Analysis. The institutional review board of the Galilee Medical Center and the Israeli Ministry of Health approved the study. All study participants and parents of minors signed informed consent forms.

Exonic sequences from the DNA sample of the patient were enriched using the SureSelect Human All Exon 50 Mb V.4 Kit (Agilent Technologies). Sequences (100-bp paired-end) were generated on a HiSeq 2000 (Illumina). Read alignment and variant calling were performed with DNAnexus using default parameters with the human genome assembly hg19 (GRCh37) as reference. Parental consent was given for DNA studies.

RFLP Analysis. DNA was extracted from whole-blood samples of 24 family members using the FlexiGene DNA Kit (QIAGEN). The first methionine-encoding region of the NME3 gene was amplified using PCR with the forward primer 5′-GGTTCCGGGGTGCAAGTGAA-3′ and the reverse primer 5′-TCGAAGCGCCGCACAATCTC-3′. The reaction was conducted using ReadyMix PCR Master Mix (Thermo Fisher Scientific) at an annealing temperature of 62 °C. PCR products (343 bp) were digested using the *FatI* restriction enzyme (New England Biolabs) according to the manufacturer's recommendations. Samples were analyzed using 3.5% agarose gel electrophoresis and ethidium bromide staining, and visualized using an ImageQuant LAS 4000 (GE Healthcare Life Sciences).

Cell Culture, Transfection, and Infection. F741 and F689 fibroblast were maintained in RPMI 1640 (11875-085; Gibco) containing 20% FBS. BJ fibroblast were maintained in RPMI 1640 medium (11875-085; Gibco) containing 10% FBS. For glucose deprivation, cells were incubated in glucose-free RPMI 1640 (11879-020; Gibco) containing 20% dialyzed FBS. HeLa and HEK293T cells were maintained in DMEM supplemented with 10% FBS, 100 U/mL penicillin, and 10 μg/mL streptomycin. For the lenti-virus package, HEK293T cells were cotransfected with pCMVdeltaR8.91, pCMV VSVG, and pAS4.1w.Pbsd-aOn-Flag-NME3 plasmids (or shRNA plasmids). After transfection for 48 and 72 h, supernatants containing lentivirus were filtered through a PVDF membrane (pore size 0.45 μm; Millipore). The siRNAs against MFN1/2 were purchased from Dharmacon (smart pool siGenome, M-010670-01 for siMFN1, M-012960-00 for siMFN2).

Plasmids and Reagents. The Tet-on expression vector of Flag-NME3 was constructed by insertion of PCR products amplified from the NME3 expression vector at NheI (5′) and PmeI (3′) of the pAS4.1w.pBsd-aOn vector. The expression vector of NME3-HA was constructed by insertion of PCR products amplified from the NME3 expression vector at KpnI (5′) and XhoI (3′) of the pCDNA3.0-HA plasmid. pET28m-6×His-thrombin-NME3-WT, -H135Q, and -E40/46D were used for protein purification of NME3. All mutations were generated by using a QuikChange XL Site-Directed Mutagenesis Kit (200522; Stratagene). Antibodies used in this study were as follows: Flag (F3165; Sigma-Aldrich), COX4 (4850; Cell Signaling), TOMM20 (ab56783; Abcam), Myc (clone 9E10; homemade), MFN1 (14739S; Cell Signaling), MFN2 (ab56889; Abcam), DRP1 (8570; Cell Signaling), OPA1 (612606; BD Biosciences), SOD2 (06-984; Millipore), MiD51 (20164-1-AP; Proteintech), MiD49 (16413-1-AP; Proteintech), MFF (17090-1-AP; Proteintech), Fis1 (10956-1-AP; Proteintech), MTHFD2 (12270-1-AP; Proteintech), HA (sc805; Santa Cruz), His (631212; Clontech), Myc (sc40; Santa Cruz), GFP (632375; Clontech), β-tubulin (T4026; Sigma-Aldrich), total OXPHOS human WB antibody mixture (ab110411; Abcam), and N1-phosphohistidine (1-pHis, MABS1341; Millipore).

Superresolution Microscopy. Direct stochastic optical reconstruction microscopy (dSTORM) was used for superresolution imaging as described previously (30). Briefly, cells expressing Flag-tagged NME3 were fixed with 4% paraformaldehyde and immunostained with antibodies of Flag (F1804; 1:300 dilution; Sigma-Aldrich), TOMM20 (ab56783; 1:200; Abcam), and COX4 (4850; 1:200; Cell Signaling). For two-color dSTORM imaging of either Flag-NME3 with TOMM20 or Flag-NME3 with COX4, Alexa Fluor 647 dye (rabbit A21245; mouse A21236; Invitrogen) and Cy3b [conjugating Cy3B maleimide (GE; PA63131) to IgG antibodies (rabbit 711-005-152; mouse 715–005-151; Jackson)] were used as secondary antibodies. Fiducial markers (Tetraspeck, T7279; Thermo Fisher Scientific) were added to the sample to correct possible mechanical drift. Alexa 647 and Cy3B were imaged sequentially with 637- and 561-nm light (2 to 5 kW/cm^2), respectively. A weak 405-nm light (<5 W/cm^2) was used to activate a portion of the probes converted from a dark state to an excitation state. The imaging buffer consisted of TN buffer (10 mM Tris-HCl, pH 8.0, and 150 mM NaCl) and an oxygen-scavenging system [60 to 100 mM mercaptoethylamine, 0.5 mg/mL glucose oxidase, 40 μg/mL catalase, and 10% (wt/vol) glucose; Sigma-Aldrich]. In general, 10,000 to 20,000 frames were recorded for each image.

Mitochondria Fractionation and Proteinase K Treatment. For mitochondria fractionation, HeLa cells washed with 10 mM Hepes (pH 7.4) were resuspended with 800 μL of homogenizing buffer (10 mM Hepes, pH 7.4, 70 mM sucrose, and 220 mM mannitol) drawing through a 27-gauge syringe needle 30 times. After centrifugation at 800 × *g* for 10 min at 4 °C, suspended lysates were centrifuged at 10,000 × *g* for 10 min at 4 °C to collect mitochondria-rich fractionation. After washing with homogenizing buffer, mitochondria were resuspended in proteinase K reaction buffer (20 mM Hepes, pH 7.4, 250 mM sucrose, 80 mM potassium acetate, and 5 mM magnesium acetate) in the presence and absence of proteinase K (20 μg/mL) at 12 °C for 30 min.

Determination of Mitochondrial Morphology and Mito-Dendra2 Photoconversion Assay. Cells were fixed with 4% paraformaldehyde at 37 °C for COX4 IF staining for morphology evaluation. To determine mitochondrial fusion, cells were transfected with the mito-Dendra2 plasmid overnight. Cells were pretreated with 30 μg/mL cycloheximide for 30 min to block new synthesis of mito-Dendra2 during time-lapse experiments. Mito-Dendra2 conversion was achieved by scanning with a 405-nm laser with 50% intensity for 50 iterations at a region of isolated mitochondria. Time-lapse recording was performed every 30 s and monitored for 20 min. Images were acquired by using a confocal fluorescence microscope (LSM780; Carl Zeiss) equipped with AxioVision Rel. 4.8 and ZEN 2009 light edition (Carl Zeiss). To quantify the extent of mitochondrial fusion, the area of converted red mito-Dendra2 overlapping with the area of non-converted green mito-Dendra2 was measured by colocalization coefficient using ZEN software (Carl Zeiss).

In Situ Proximal Ligation Assay. An in situ PLA kit was obtained from Sigma-Aldrich for the assay. Cells on coverslips were washed with Tris-buffered saline with 0.1% Triton X-100 (TBST) for 5 min twice and then incubated with the primary antibodies. Afterward, the PLA anti-mouse PLUS probe (DUO92001; Sigma-Aldrich) and anti-rabbit MINUS probe (DUO92005; Sigma-Aldrich) were incubated for 1 h at 37 °C. Cells were washed with TBST for 5 min twice and subjected to the ligation reaction for 30 min at 37 °C, followed by the amplification reaction for 90 min at 37 °C. Hoechst 33342 was added for DNA staining. Images were obtained by using fluorescence microscopy (AxioObserver A1; Carl Zeiss). AxioVision Rel. 4.8 and ImageJ (supplier set 1.44p; NIH) were used for image quantification and analysis.

NME3 Purification, NDPK Activity Assay, and Oligomerization. *Escherichia coli* BL21(DE3) cells were transformed with plasmids encoding WT-, HQ-, or E40/46D-NME3. Protein synthesis was induced by addition of 0.5 mM isopropyl β-D-1-thiogalactopyranoside at OD_{600} 0.6 and cells were harvested at OD_{600} 1.4 and resuspended in the lysis buffer containing 20 mM Tris·HCl (pH 8.0), 500 mM NaCl, 5 mM imidazole, and 1 mM β-mercaptoethanol. All protein samples were purified using affinity purification on nickel-charged Sepharose Fast Flow resin (Clontech). NDPK activity of purified NME3 was measured by luciferase-coupled assay. Protein in 20 μL was incubated in 15 μL of the reaction buffer containing 100 mM Tris·HCl (pH 8.0), 100 mM KCl, 10 mM $MgCl_2$, 50 μM ADP, and 50 μM UDP for 10 min, followed by addition of 15 μL of Kinase-Glo (Promega) for detecting ATP production. Bioluminescence was measured by the TECAN SPARK System. For oligomerization analysis, purified protein was incubated with 10 mM bismaleimidohexane (BMH; 22330; Thermo Fisher Scientific) for 30 min at room temperature, followed by addition of β-mercaptoethanol to 0.4%. After heating, samples were separated by using 4 to 12% Bis-Tris gradient gels (MAN0007891; Life Technologies) with NuPAGE running buffer according to instructions by the manufacturer.

Electron Microscopy of Mitochondrial Morphology. Cultures were washed with 0.1 M PBS twice and then were detached with 0.05% trypsin-EDTA. Cells were further pelletted by centrifugation at 845 × *g* for 5 min. The pellet was resuspended and fixed in 5% glutaraldehyde for 2 h at 4 °C and postfixed in 2% osmic acid for 2 h at room temperature, dehydrated, and embedded in Epon 812 resin (Polysciences). Ultrathin (70-nm) sections were stained with uranyl acetate and lead citrate and observed under a transmission electron microscope (H7100; Hitachi). Seventeen to 27 fields with mitochondria were randomly photographed at an original magnification of 50,000×, and mitochondria ($n > 50$ in each group) were analyzed in a blinded setting. All cristae in the entire mitochondria were counted, and the mitochondrial area was measured by Image-Pro Plus software (Media Cybernetics).

Mitochondrial DNA Copy Number. DNA was extracted with the Wizard Genomic DNA Purification Kit (A1125; Promega). After protein precipitation, samples were combined with an equal volume of isopropanol for DNA precipitation. Extracted DNA samples were rehydrated and analyzed by quantitative real-time PCR using the ABI StepOne System (Applied Biosystems) with Fast SYBR Green PCR Master Mix (Kapa Biosystems). Primers for mitochondrial DNA (*mitochondria encoded NADH dehydrogenase 1* gene; *MT-ND1*) and for the nuclear *GAPDH* gene were used for each sample. The primer for *MT-ND1* (mtDNA) was 5′-GCTACTACAACCCTTCGCTGAC-3′, and for *GAPDH* (nuclear DNA) was 5′-CAGGACCCCACAGCCGACCT-3′. The copy number of mitochondrial DNA was normalized by the amount of nuclear DNA by using the double-delta CT method.

Oxygen Consumption Rate and Mitochondrial Oxidative Stress Measurement. Cells plated in XF 24-well cell-culture microplates (Seahorse Bioscience) at a density of 6,000 cells per well were incubated in 675 μL of bicarbonate-free growth medium at 37 °C without 5% CO_2 for 1 h before starting OCR measurement by XFe24 Extracellular Flux Analyzer (Seahorse Bioscience, Agilent Technologies). OCR was measured under basal conditions and followed by the addition of 1 μM oligomycin, 1 μM carbonyl cyanide 4-(trifluoromethoxy)phenylhydrazone (FCCP), and 0.5 μM rotenone/antimycin A. The cell number of each well was counted after OCR measurement for normalization. Data were expressed as pmol of O_2 per min in 6,000 cells. Mitochondrial superoxide was measured by incubated cells with MitoSOX red indicator (3.75 μM; M36008; Thermo Fisher Scientific) for 10 min at 37 °C. Cells were fixed with 4% paraformaldehyde in PBS for 15 min at room temperature, and images were acquired with a Carl Zeiss AxioObserver A1 with 63× oil objective.

Cellular ATP Determination. The cellular level of ATP was determined by CellTiter-Glo Luminescent Cell Viability Assay (G7571; Promega) according to the manufacturer's instructions. Briefly, 200 μL of CellTiter-Glo Reagent was directly added to 200 μL of PBS containing 5,000 suspended cells. After 10 min of incubation at room temperature, luminescence signal was measured using the TECAN SPARK System. The amount of cellular ATP was calculated from interpolation of the ATP standard curve.

Detection of Histidine Phosphorylation. Cells were directly harvested by SDS/PAGE sample buffer (100 mM Tris·HCl, pH 8.8, 4% SDS, 0.008% bromophenol blue, 20% glycerol, 20 mM EDTA, and 200 mM DTT), followed by sonication and centrifugation at 10,000 × *g* for 25 min at 4 °C. Samples were divided into two parts: with and without incubation at 95 °C for 10 min. SDS/PAGE was modified using a 3% stacking gel (pH 8.8) and 10% resolving gel. After the electrophoresis step, the protein gel was transferred onto a PVDF membrane at 60 V for 3 h and another 80 V for 2 h at 4 °C for Western blotting by using 1-pHis monoclonal antibody (MABS1341; Millipore).

Statistical Analysis. All values are presented as mean ± SD or SEM as indicated. Statistical analysis of the results from three independent experiments was performed by Student's *t* test (two-tailed). A *P* value of less than 0.05 was considered statistically significant.

ACKNOWLEDGMENTS. We thank the National RNAi Core Facility, Academia Sinica for their help in providing shRNA plasmids and Tet-on plasmids. We thank the staff of the imaging core at the First Core Labs, National Taiwan University College of Medicine for technical assistance. This research is supported by grants from the Ministry of Science and Technology, Taiwan (MOST 107-3017-F-002-002 and MOST 107-2321-B-002-041).

1. Takács-Vellai K, Vellai T, Farkas Z, Mehta A (2015) Nucleoside diphosphate kinases (NDPKs) in animal development. *Cell Mol Life Sci* 72:1447–1462.
2. Boissan M, et al. (2009) The mammalian Nm23/NDPK family: From metastasis control to cilia movement. *Mol Cell Biochem* 329:51–62.
3. Lacombe ML, Milon L, Munier A, Mehus JG, Lambeth DO (2000) The human Nm23/nucleoside diphosphate kinases. *J Bioenerg Biomembr* 32:247–258.
4. Boissan M, et al. (2014) Membrane trafficking. Nucleoside diphosphate kinases fuel dynamin superfamily proteins with GTP for membrane remodeling. *Science* 344: 1510–1515.
5. Abu-Taha IH, et al. (2017) Nucleoside diphosphate kinase-C suppresses cAMP formation in human heart failure. *Circulation* 135:881–897.
6. Okamoto K, Shaw JM (2005) Mitochondrial morphology and dynamics in yeast and multicellular eukaryotes. *Annu Rev Genet* 39:503–536.
7. Mishra P, Chan DC (2016) Metabolic regulation of mitochondrial dynamics. *J Cell Biol* 212:379–387.
8. Chen H, Chomyn A, Chan DC (2005) Disruption of fusion results in mitochondrial heterogeneity and dysfunction. *J Biol Chem* 280:26185–26192.
9. Ishihara N, Eura Y, Mihara K (2004) Mitofusin 1 and 2 play distinct roles in mitochondrial fusion reactions via GTPase activity. *J Cell Sci* 117:6535–6546.
10. Chen H, et al. (2003) Mitofusins Mfn1 and Mfn2 coordinately regulate mitochondrial fusion and are essential for embryonic development. *J Cell Biol* 160:189–200.
11. Edvardson S, et al. (2016) A mutation in the THG1L gene in a family with cerebellar ataxia and developmental delay. *Neurogenetics* 17:219–225.
12. Chen H, McCaffery JM, Chan DC (2007) Mitochondrial fusion protects against neurodegeneration in the cerebellum. *Cell* 130:548–562.
13. Gomes LC, Di Benedetto G, Scorrano L (2011) During autophagy mitochondria elongate, are spared from degradation and sustain cell viability. *Nat Cell Biol* 13:589–598.
14. Rambold AS, Kostelecky B, Elia N, Lippincott-Schwartz J (2011) Tubular network formation protects mitochondria from autophagosomal degradation during nutrient starvation. *Proc Natl Acad Sci USA* 108:10190–10195.
15. Lee JY, et al. (2014) MFN1 deacetylation activates adaptive mitochondrial fusion and protects metabolically challenged mitochondria. *J Cell Sci* 127:4954–4963.
16. Schlattner U, et al. (2018) NME4/nucleoside diphosphate kinase D in cardiolipin signaling and mitophagy. *Lab Invest* 98:228–232.
17. Karbowski M, et al. (2004) Quantitation of mitochondrial dynamics by photolabeling of individual organelles shows that mitochondrial fusion is blocked during the Bax activation phase of apoptosis. *J Cell Biol* 164:493–499.
18. Chan DC (2012) Fusion and fission: Interlinked processes critical for mitochondrial health. *Annu Rev Genet* 46:265–287.
19. Moullan N, et al. (2015) Tetracyclines disturb mitochondrial function across eukaryotic models: A call for caution in biomedical research. *Cell Rep* 10:1681–1691.
20. Schrepfer E, Scorrano L (2016) Mitofusins, from mitochondria to metabolism. *Mol Cell* 61:683–694.
21. Cogliati S, et al. (2013) Mitochondrial cristae shape determines respiratory chain supercomplexes assembly and respiratory efficiency. *Cell* 155:160–171.
22. Zorzano A, Liesa M, Sebastián D, Segalés J, Palacín M (2010) Mitochondrial fusion proteins: Dual regulators of morphology and metabolism. *Semin Cell Dev Biol* 21: 566–574.
23. Jiang M, et al. (2017) Increased total mtDNA copy number cures male infertility despite unaltered mtDNA mutation load. *Cell Metab* 26:429–436.e4.
24. Fuhs SR, et al. (2015) Monoclonal 1- and 3-phosphohistidine antibodies: New tools to study histidine phosphorylation. *Cell* 162:198–210.
25. Seo AY, et al. (2017) AMPK and vacuole-associated Atg14p orchestrate μ-lipophagy for energy production and long-term survival under glucose starvation. *eLife* 6: e21690.
26. Rambold AS, Cohen S, Lippincott-Schwartz J (2015) Fatty acid trafficking in starved cells: Regulation by lipid droplet lipolysis, autophagy, and mitochondrial fusion dynamics. *Dev Cell* 32:678–692.
27. Fuhs SR, Hunter T (2017) pHisphorylation: The emergence of histidine phosphorylation as a reversible regulatory modification. *Curr Opin Cell Biol* 45:8–16.
28. Cagalinec M, et al. (2013) Principles of the mitochondrial fusion and fission cycle in neurons. *J Cell Sci* 126:2187–2197.
29. Nowakowska-Kotas M, Kędzia A, Dudek K (2014) Development of external surfaces of human cerebellar lobes in the fetal period. *Cerebellum* 13:541–548.
30. Yang TT, Chong WM, Liao JC (2016) STED and STORM superresolution imaging of primary cilia. *Methods Mol Biol* 1454:169–192.